An Innovative Material-by-Design Method for the Enhancement of Linear Active Electronically-Scanned Arrays

M. Salucci, G. Oliveri, N. Anselmi, G. Gottardi, and A. Massa

Abstract

The problem of enhancing the radiation features (in terms of directivity and side-lobe level) of an existing linear active electronically-scanned array (*AESA*) is addressed. A novel material-by-design (*MbD*) design technique is proposed to synthesize suitably engineered meta-material lenses able to significantly improve the performance of the covered antenna array without increasing the number of elementary radiators nor re-designing the feeding network. Moreover, the synthesized architectures are able to mimic the radiation characteristics of larger apertures without requiring highly-anisotropic meta-materials thanks to the exploitation of a customized quasi-conformal transformation optics (*QCTO*) technique in combination with a source inversion (*SI*) strategy. Some numerical results are presented and discussed in order to verify the potentialities of the proposed synthesis technique.

1 Extensive Analysis - Half-Cosine Profile - $h' = 6.0$ [λ], $l' = 0.0$ [λ], $t' = 24.0$ [λ], $N = 22$

1.1 Step 1: Expanding the physical array ($N = 22$, $L = 10.5$ [λ])

Input Parameters

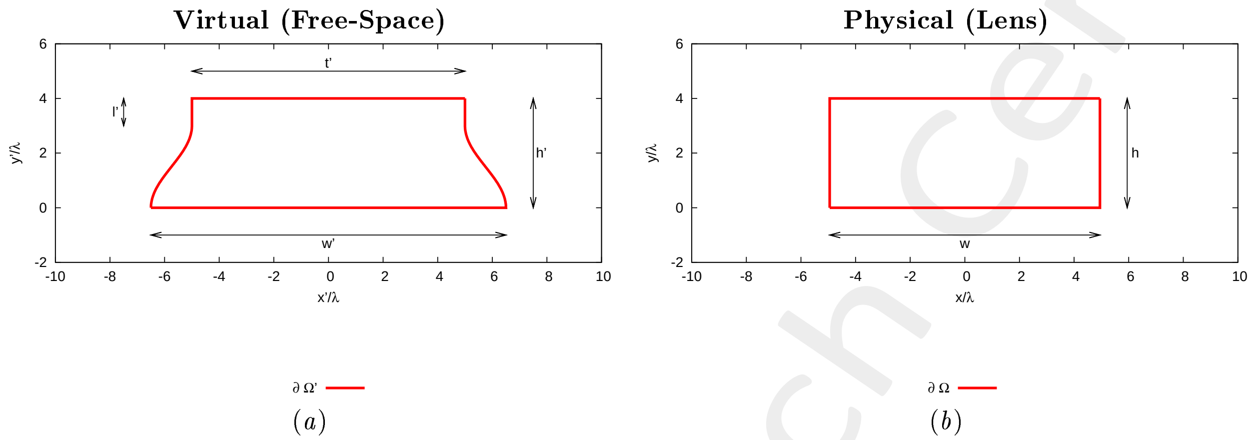

Figure 1: Transformation regions. The lower side of both virtual and physical boundaries are supposed to be PEC.

- **Virtual Geometry**

# Test Case	h' [λ]	l' [λ]	t' [λ]	w' [λ]
1	6.0	0.0	24.0	**26.7**
2	6.0	0.0	24.0	**28.5**
3	6.0	0.0	24.0	**29.7**
4	6.0	0.0	24.0	**31.05**
5	6.0	0.0	24.0	**32.1**

Table I: Considered virtual geometries. The values of w' have been empirically determined in order to achieve an aperture of the virtual array (L') equal to a multiple of $\lambda/2$. It is imposed that $h = h'$, while w is not controlled by the user.

- **Physical Array**
  - Number of elements, spacing, aperture: $N = 22$, $d = \frac{\lambda}{2}$, $L = 10.5$ [λ];
  - Positions: $x_n \in [-L/2, L/2]$, $y_n = \frac{\lambda}{4}$, $n = 1, ..., N$;
  - Excitations: $I_n = 1.0$, $\varphi_n = \frac{-2\pi}{\lambda} x_n sin(\phi_s + 90)$; $n = 1, ..., N$;
- **QCTO**
  - Discretization cell dimension: 0.05 [λ] (0.01 [λ] for source mapping);

1.1.1 Results

Resulting aperture of the virtual array (L') - for step 2

- The aperture of the virtual array (L') is computed after mapping the physical array into the virtual space;
- The resulting number of equi-spaced elements is computed as

$$N' = round\left(\frac{L'}{0.5} + 1\right)$$

	Virtual Geometry				
# Test Case	h' [λ]	l' [λ]	t' [λ]	w' [λ]	N'
1	6.0	0.0	24.0	**26.7**	**23**
2	6.0	0.0	24.0	**28.5**	**25**
3	6.0	0.0	24.0	**29.7**	**26**
4	6.0	0.0	24.0	**31.05**	**28**
5	6.0	0.0	24.0	**32.1**	**30**

Table II: Resulting aperture and number of equi-spaced elements of the virtual array after expanding the physical array.

1.2 Step 2: Compressing the virtual array ($N' > N$, $L' > L$ [λ])

Input Parameters

- **Virtual Array**
  - Number of elements, spacing, aperture: $N' = \{23; 25; 26; 28; 30\}$, $d' = \frac{\lambda}{2}$, $L' = \{11.0; 12.0; 12.5; 13.5; 14.5\}$ [λ];
  - Positions: $x'_n \in [-L'/2, L'/2]$, $y'_n = \lambda/4$, $n = 1, ..., N'$;
  - Steering angle: $\phi_s = 90$ [deg];
  - Excitations: $I'_n = 1.0$, $\varphi'_n = \frac{-2\pi}{\lambda} x_n sin\,(\phi_s + 90)$; $n = 1, ..., N'$;
- **Virtual Geometry:** same of step 1;
- **QCTO:** same of step 1.

1.3 Source Inversion (SI)

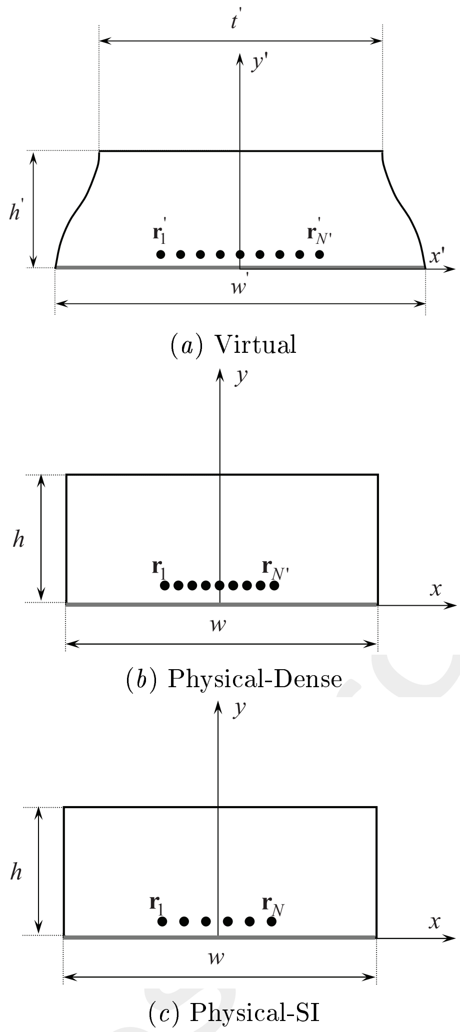

Figure 2: Geometry for (a) the virtual array in free-space, (b) the "physical-dense" array inside the lens and (c) the physical-SI array inside the lens.

Parameters

- Before SI
  - Number of elements: $N' = \{23; 25; 26; 28; 30\}$, $d' < \lambda/2$;
- After SI
  - Number of elements after SI: $N = 22$, $d = \frac{\lambda}{2}$;
  - Aperture: $L = 10.5$;
- Radius of the observation domain: $r_{SI} = 400$ $[\lambda]$;
- Number of field sampling points: $n_{SI} = 1000$.

1.3.1 Near-Field Distribution ($\phi_s = 90$ [deg], $f = 600$ [MHz])

Case $w' = 26.7$ [λ], $N = 22 \rightarrow N' = 23$

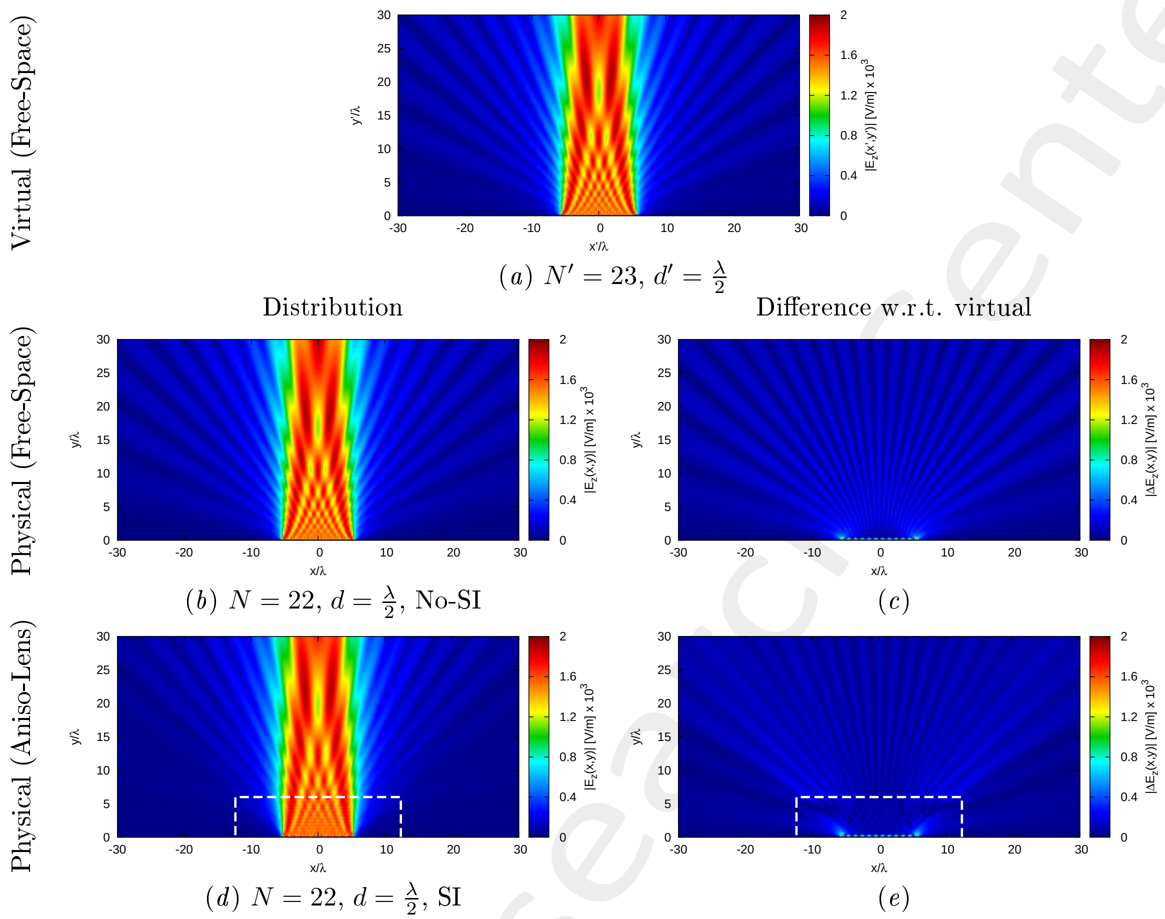

(a) $N' = 23$, $d' = \frac{\lambda}{2}$

(b) $N = 22$, $d = \frac{\lambda}{2}$, No-SI

(c)

(d) $N = 22$, $d = \frac{\lambda}{2}$, SI

(e)

Figure 3: $\phi_s = 90$ [deg], $f = 600$ [MHz] - Electric field distributions.

Case $w' = 28.5$ **[λ],** $N = 22 \rightarrow N' = 25$

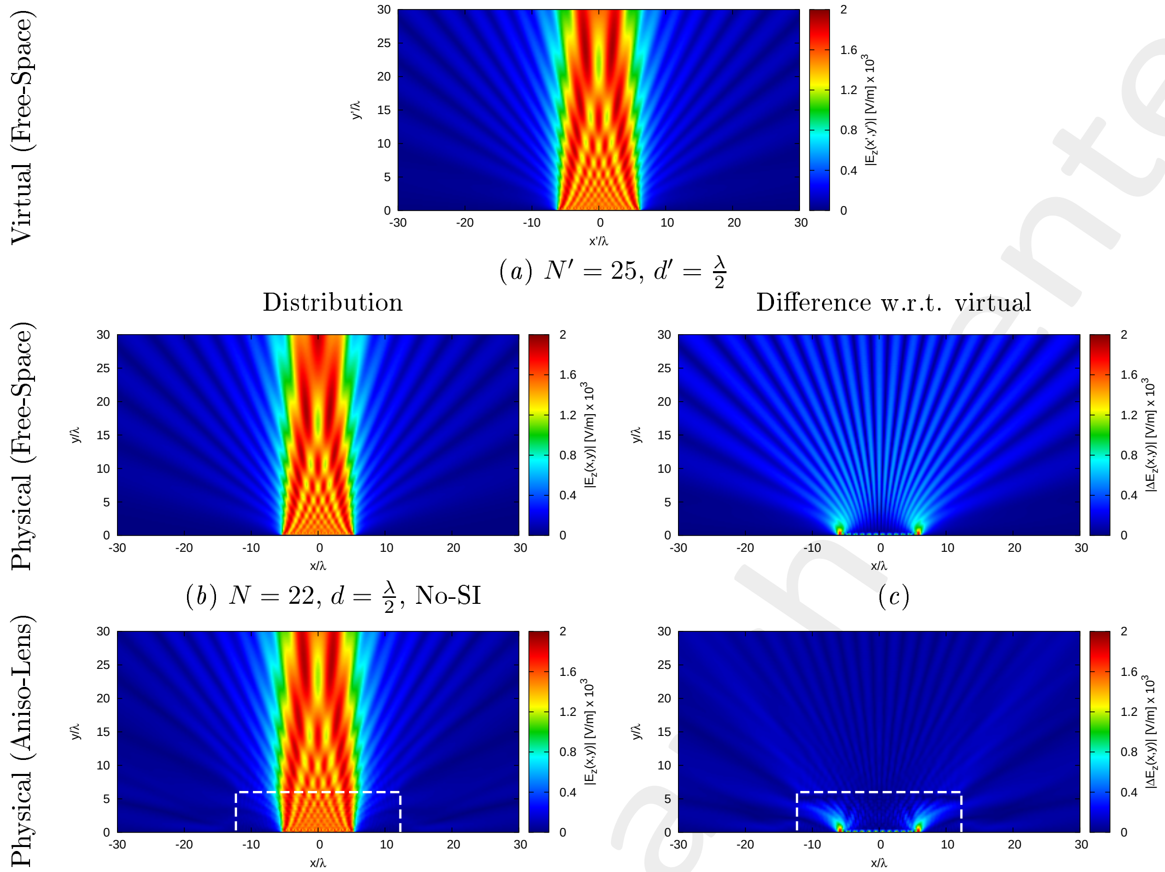

(a) $N' = 25$, $d' = \frac{\lambda}{2}$

(b) $N = 22$, $d = \frac{\lambda}{2}$, No-SI (c)

(d) $N = 22$, $d = \frac{\lambda}{2}$, SI (e)

Figure 4: $\phi_s = 90$ [deg], $f = 600$ [MHz] - Electric field distributions.

Case $w' = 29.7$ **[**λ**],** $N = 22 \rightarrow N' = 26$

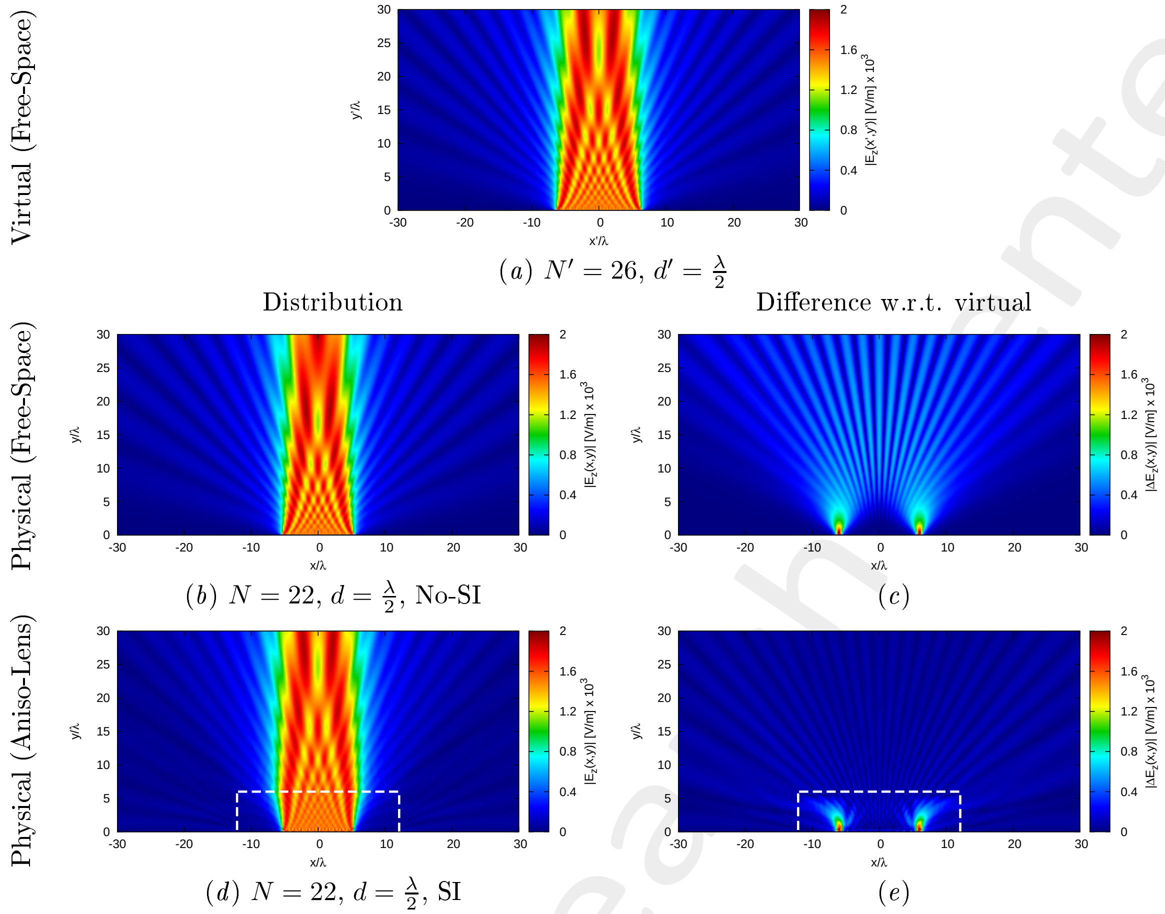

Figure 5: $\phi_s = 90$ [deg], $f = 600$ [MHz] - Electric field distributions.

Case $w' = 31.05$ **[λ],** $N = 22 \rightarrow N' = 28$

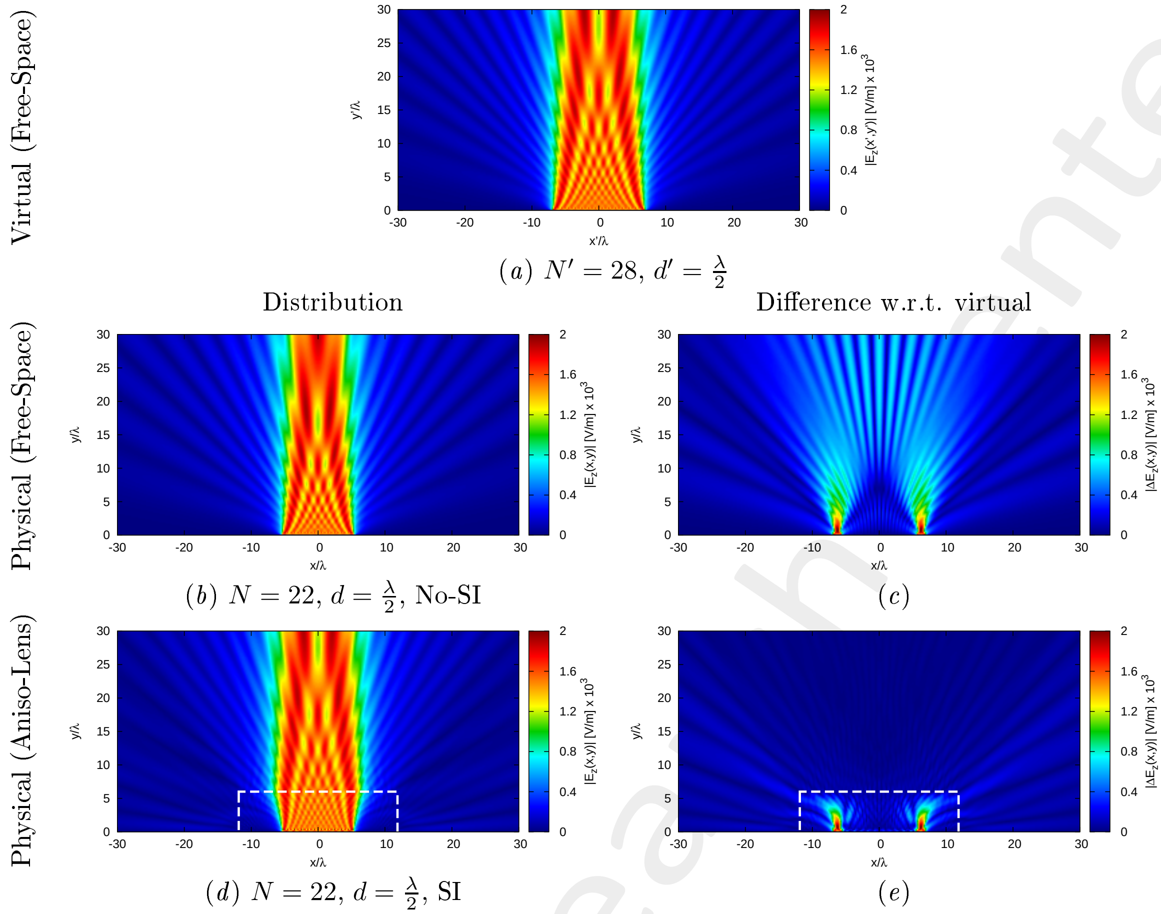

Figure 6: $\phi_s = 90$ [deg], $f = 600$ [MHz] - Electric field distributions.

Case $w' = 32.1$ **[**λ**]**, $N = 22 \rightarrow N' = 30$

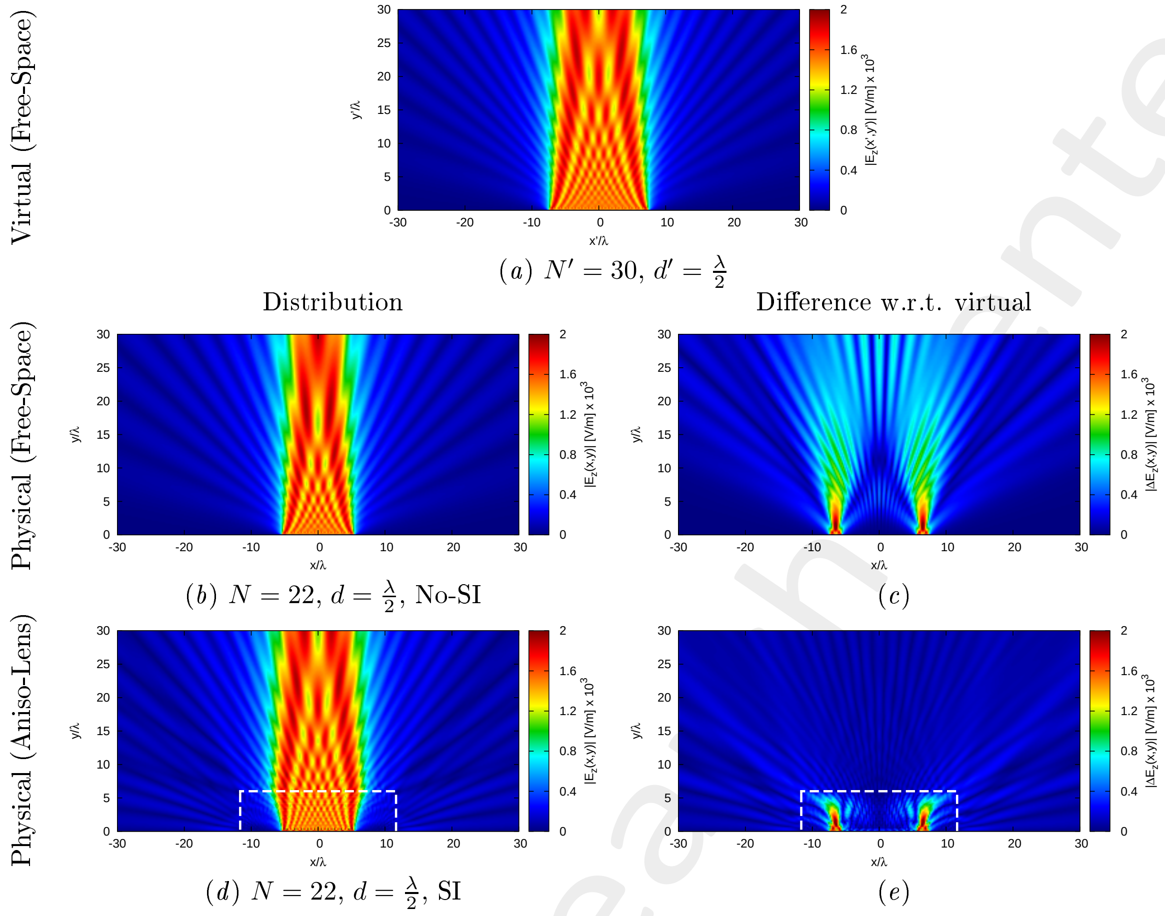

Figure 7: $\phi_s = 90$ [deg], $f = 600$ [MHz] - Electric field distributions.

1.3.2 Far-Field Patterns ($\phi_s = 90$ [deg], $f = 600$ [MHz])

Anisotropic Lens

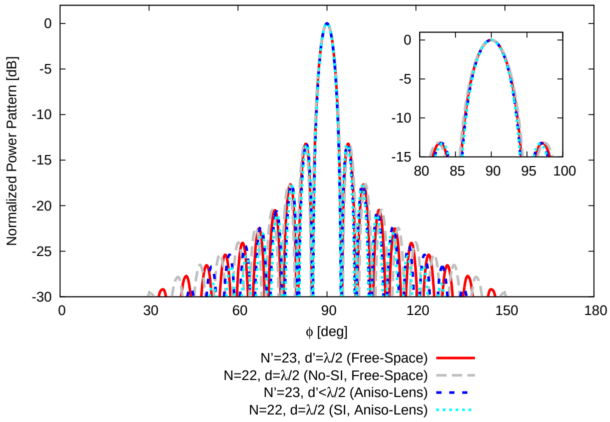

(a) $w' = 26.7$ [λ], $N' = 23$

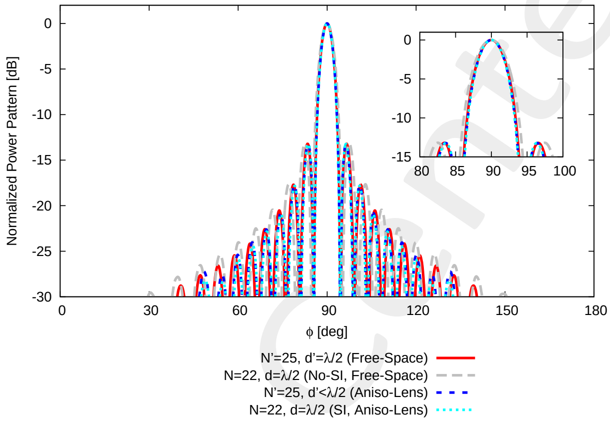

(b) $w' = 28.5$ [λ], $N' = 25$

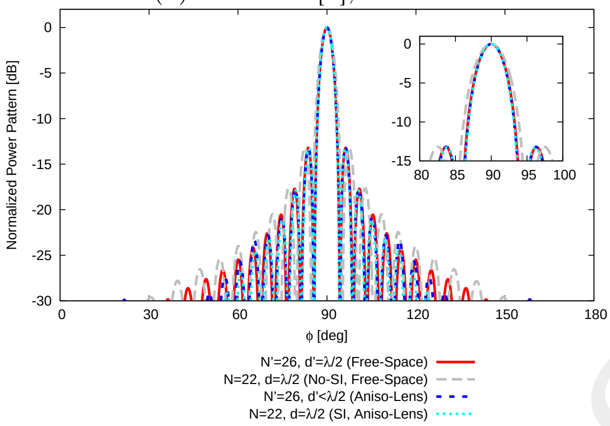

(c) $w' = 29.7$ [λ], $N' = 26$

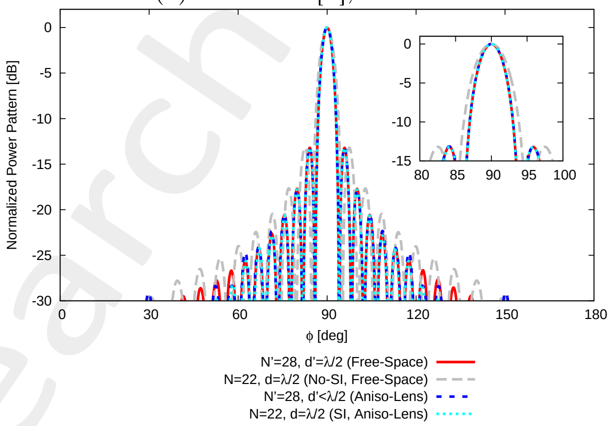

(d) $w' = 31.05$ [λ], $N' = 28$

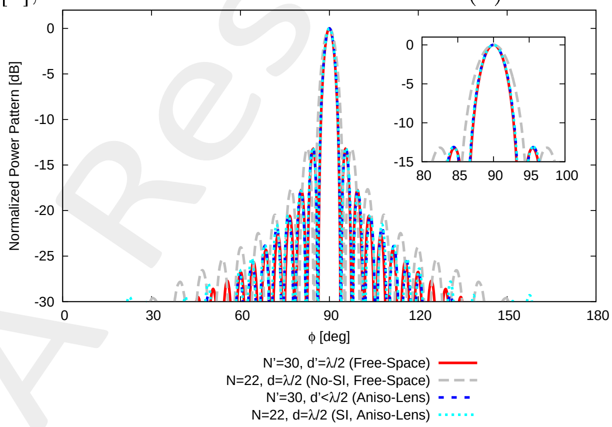

(e) $w' = 32.1$ [λ], $N' = 30$

Figure 8: $\phi_s = 90$ [deg], $f = 600$ [MHz] - Far field pattern comparison for different values of w'.

1.3.3 Final Summary ($f = 600$ [MHz])

Test Case 1 - $w' = 26.7$ [λ], $N = 22 \rightarrow N' = 23$

	Virtual Array	**Physical "Dense" Array**			**Physical-SI Array**		
Environment	Free-Space	Free-Space	Aniso-Lens	Iso-Lens	Free-Space (No-SI)	Aniso-Lens (SI)	Iso-Lens (SI)
Number of elements	23	23			22		
Aperture [λ]	11.0	10.23			10.5		
Spacing [λ]	0.5	< 0.5			0.5		
Aperture Ratio (w.r.t. virtual)	-	0.93			0.95		
	Steering at $\phi_s = 90$ [deg], $f = 600$ [MHz]						
SLL [dB]	13.21	13.19	13.25	-	13.20	13.30	-
$FNBW$ [deg]	9.99	10.71	9.63	-	10.35	9.45	-
$HPBW$ [deg]	4.41	4.74	4.29	-	4.61	4.23	-
$D_{\max}$ [dB]	15.57	15.26	15.70	-	15.37	15.80	-
Matching Error, ξ (w.r.t. virtual, outside lens)	-	4.10×10^{-1}	2.14×10^{-1}	-	2.66×10^{-1}	2.40×10^{-1}	-

Table III: Test case 1 - $w^{'} = 26.7$ [λ]: Summary.

Test Case 2 - $w' = 28.5$ [λ], $N = 22 \rightarrow N' = 25$

	Virtual Array	Physical "Dense" Array			Physical-SI Array		
Environment	Free-Space	Free-Space	Aniso-Lens	Iso-Lens	Free-Space (No-SI)	Aniso-Lens (SI)	Iso-Lens (SI)
Number of elements	25	22			22		
Aperture [λ]	12.00	10.41			10.5		
Spacing [λ]	0.5	< 0.5			0.5		
Aperture Ratio (w.r.t. virtual)	-	0.87			0.875		
	Steering at $\phi_s = 90$ [deg], $f = 600$ [MHz]						
SLL [dB]	13.21	13.22	13.22	-	13.20	13.23	-
$FNBW$ [deg]	9.09	10.53	8.91	-	10.35	8.91	-
$HPBW$ [deg]	4.05	4.67	3.94	-	4.61	3.91	-
$D_{\max}$ [dB]	15.93	15.32	16.06	-	15.37	16.11	-
Matching Error, ξ (w.r.t. virtual, outside lens)	-	5.92×10^{-1}	1.82×10^{-1}	-	5.47×10^{-1}	1.99×10^{-1}	-

Table IV: Test case 2 - $w^{'} = 28.5$ [λ]: Summary.

Test Case 3 - $w' = 29.7$ [λ], $N = 22 \rightarrow N' = 26$

	Virtual Array	**Physical "Dense" Array**			**Physical-SI Array**		
Environment	Free-Space	Free-Space	Aniso-Lens	Iso-Lens	Free-Space (No-SI)	Aniso-Lens (SI)	Iso-Lens (SI)
Number of elements	26	26			22		
Aperture [λ]	12.5	10.28			10.5		
Spacing [λ]	0.5	< 0.5			0.5		
Aperture Ratio (w.r.t. virtual)	-	0.822			0.84		
	Steering at $\phi_s = 90$ [deg], $f = 600$ [MHz]						
SLL [dB]	13.21	13.23	13.20	-	13.20	13.27	-
$FNBW$ [deg]	8.73	10.71	8.73	-	10.35	8.55	-
$HPBW$ [deg]	3.90	4.74	3.81	-	4.61	3.78	-
$D_{\max}$ [dB]	16.10	15.27	16.19	-	15.37	16.27	-
Matching Error, ξ (w.r.t. virtual, outside lens)	-	6.00×10^{-1}	1.15×10^{-1}	-	5.56×10^{-1}	1.58×10^{-1}	-

Table V: Test case 3 - $w^{'} = 29.7$ [λ]: Summary.

Test Case 4 - $w' = 31.05$ [λ], $N = 22 \rightarrow N' = 28$

	Virtual Array	Physical "Dense" Array			Physical-SI Array		
Environment	Free-Space	Free-Space	Aniso-Lens	Iso-Lens	Free-Space (No-SI)	Aniso-Lens (SI)	Iso-Lens (SI)
Number of elements	28	28			22		
Aperture [λ]	13.5	10.42			10.5		
Spacing [λ]	0.5	< 0.5			0.5		
Aperture Ratio (w.r.t. virtual)	-	0.771			0.778		
	Steering at $\phi_s = 90$ [deg], $f = 600$ [MHz]						
SLL [dB]	13.21	13.21	13.15	-	13.20	13.20	-
$FNBW$ [deg]	8.19	10.53	8.19	-	10.35	8.19	-
$HPBW$ [deg]	3.62	4.69	3.65	-	4.61	3.62	-
$D_{\max}$ [dB]	16.42	15.32	16.39	-	15.37	16.44	-
Matching Error, ξ (w.r.t. virtual, outside lens)	-	6.91×10^{-1}	1.38×10^{-1}	-	6.05×10^{-1}	1.31×10^{-1}	-

Table VI: Test case 4 - $w^{'} = 31.05$ [λ]: Summary.

Test Case 5 - $w' = 32.1$ [λ], $N = 22 \rightarrow N' = 30$

	Virtual Array	**Physical "Dense" Array**			**Physical-SI Array**		
Environment	Free-Space	Free-Space	Aniso-Lens	Iso-Lens	Free-Space (No-SI)	Aniso-Lens (SI)	Iso-Lens (SI)
Number of elements	30	30			22		
Aperture [λ]	14.5	10.64			10.5		
Spacing [λ]	0.5	< 0.5			0.5		
Aperture Ratio (w.r.t. virtual)	-	0.73			0.72		
	Steering at $\phi_s = 90$ [deg], $f = 600$ [MHz]						
SLL [dB]	13.23	13.24	13.12	-	13.20	13.09	-
$FNBW$ [deg]	7.65	10.35	7.83	-	10.35	7.83	-
$HPBW$ [deg]	3.38	4.61	3.46	-	4.61	3.48	-
$D_{\max}$ [dB]	16.72	15.40	16.61	-	15.37	16.57	-
Matching Error, ξ (w.r.t. virtual, outside lens)	-	7.33×10^{-1}	2.17×10^{-1}	-	6.43×10^{-1}	2.44×10^{-1}	-

Table VII: Test case 5 - $w^{'} = 32.1$ [λ]: Summary.

1.3.4 Final Summary: Performances vs. w' (vs. N')

Steering at $\phi_s = 90$ [deg]

This figure compares the pattern characteristics of

1. Original array ($N = 22$ elements, $d = \lambda/2$, Free-Space) - GREY;
2. Target array ($N' > N$ elements, $d = \lambda/2$, Free-Space) - RED;
3. QCTO-SI array ($N = 22$ elements, $d = \lambda/2$, Anisotropic Lens + SI) - CYAN;

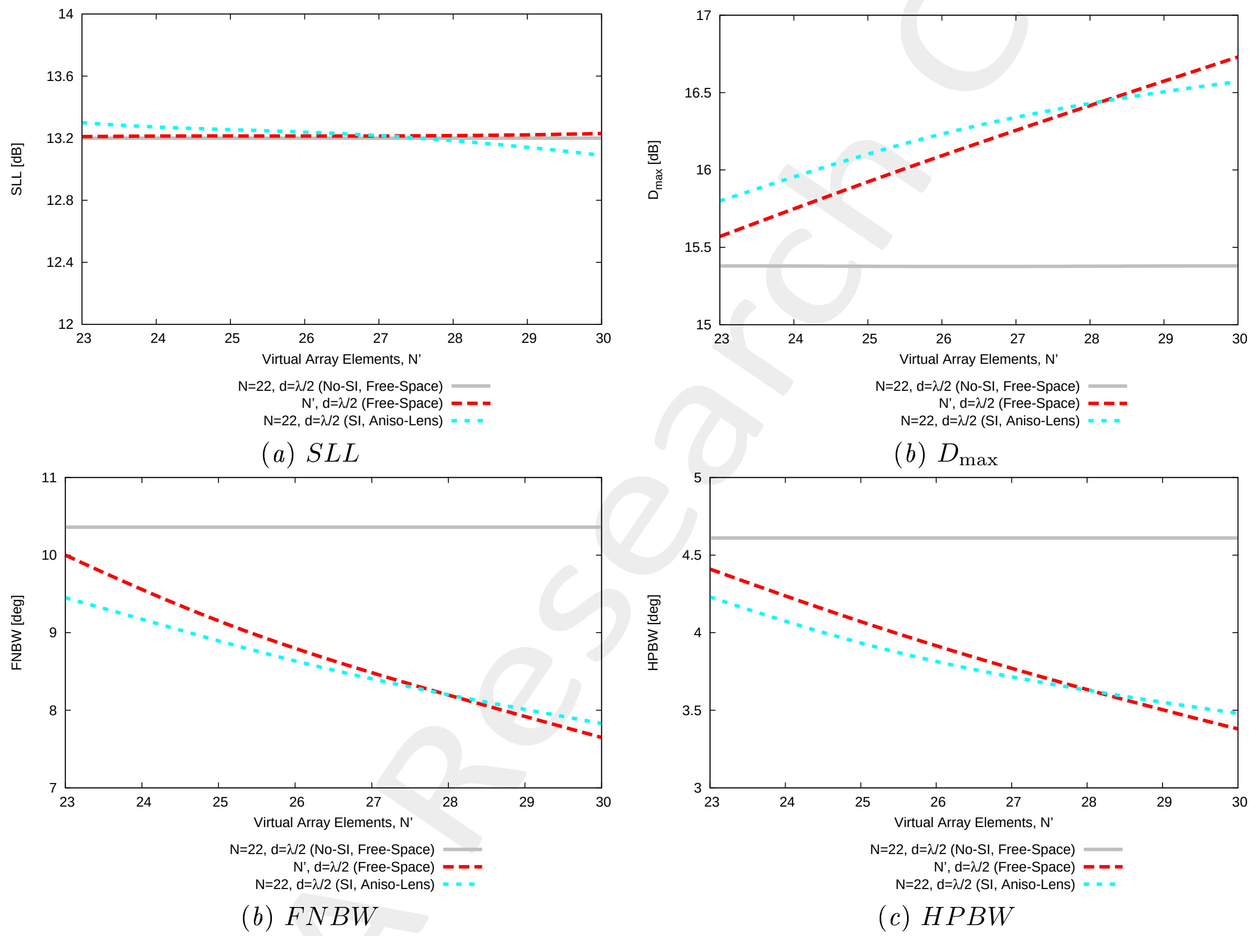

(a) *SLL* (b) $D_{\max}$ (b) *FNBW* (c) *HPBW*

Figure 9: Aniso-Lens, $f = 600$ [MHz] - Pattern performances vs w' (vs. N').

1.3.5 Physical Array with SI ($N = 22$): Achievable Performances (Anisotropic Lens)

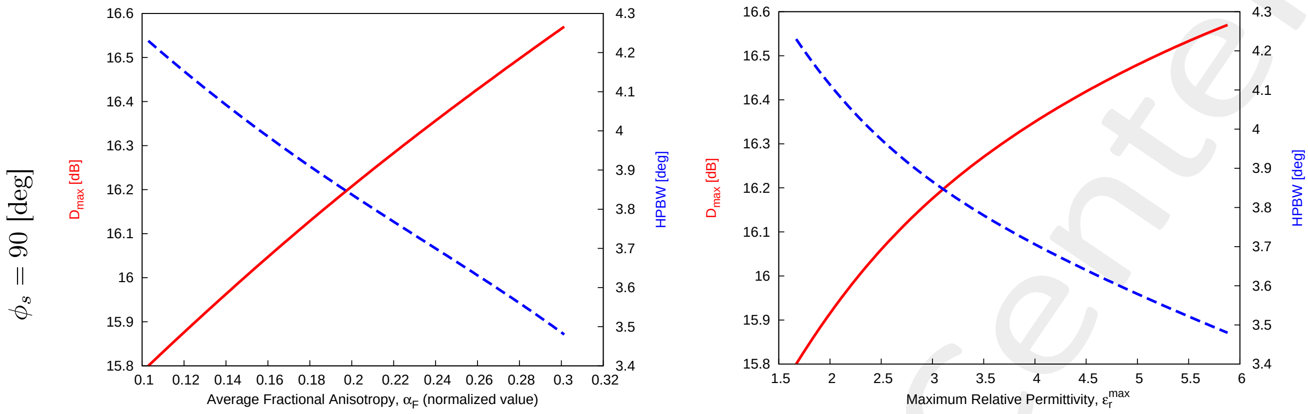

(a) (b)

Figure 10: Maximum directivity ($D_{\max}$) and $HPBW$ of the physical array with $N = 22$ elements (after SI and inside the anisotropic lens) vs. anisotropy of the lens and its permittivity ranges, for different steering angles (ϕ_s).

References

[1] G. Oliveri, G. Gottardi, F. Robol, A. Polo, L. Poli, M. Salucci, M. Chuan, C. Massagrande, P. Vinetti, M. Mattivi, R. Lombardi, and A. Massa, "Co-design of unconventional array architectures and antenna elements for 5G base station," *IEEE Trans. Antennas Propag.*, vol. 65, no. 12, pp. 6752-6767, Dec. 2017.

[2] P. Rocca, G. Oliveri, R. J. Mailloux, and A. Massa, "Unconventional phased array architectures and design methodologies - A review," *Proc. IEEE*, vol. 104, no. 3, pp. 544-560, Mar. 2016.

[3] G. Oliveri, M. Salucci, N. Anselmi and A. Massa, "Multiscale System-by-Design synthesis of printed WAIMs for waveguide array enhancement," *IEEE J. Multiscale Multiphysics Computat. Techn.*, vol. 2, pp. 84-96, 2017.

[4] A. Massa and G. Oliveri, "Metamaterial-by-Design: Theory, methods, and applications to communications and sensing - Editorial," *EPJ Applied Metamaterials*, vol. 3, no. E1, pp. 1-3, 2016.

[5] L. Poli, G. Oliveri, P. Rocca, M. Salucci, and A. Massa, "Long-Distance WPT Unconventional Arrays Synthesis," *J. Electromagnet. Wave.*, vol. 31, no. 14, pp. 1399-1420, Jul. 2017.

[6] G. Oliveri, F. Viani, N. Anselmi, and A. Massa, "Synthesis of multi-layer WAIM coatings for planar phased arrays within the system-by-design framework," *IEEE Trans. Antennas Propag.*, vol. 63, no. 6, pp. 2482-2496, Jun. 2015.

[7] G. Oliveri, L. Tenuti, E. Bekele, M. Carlin, and A. Massa, "An SbD-QCTO approach to the synthesis of isotropic metamaterial lenses," *IEEE Antennas Wireless Propag. Lett.*, vol. 13, pp. 1783-1786, 2014.

[8] G. Oliveri, D. H. Werner, and A. Massa, "Reconfigurable electromagnetics through metamaterials - A review" *Proc. IEEE*, vol. 103, no. 7, pp. 1034-1056, Jul. 2015.

[9] G. Oliveri, E. T. Bekele, M. Salucci, and A. Massa, "Transformation electromagnetics miniaturization of sectoral and conical horn antennas," *IEEE Trans. Antennas Propag.*, vol. 64, no. 4, pp. 1508-1513, Apr. 2016.

[10] G. Oliveri, E. T. Bekele, M. Salucci, and A. Massa, "Array miniaturization through QCTO-SI metamaterial radomes," *IEEE Trans. Antennas Propag.*, vol. 63, no. 8, pp. 3465-3476, Aug. 2015.

[11] G. Oliveri, E. T. Bekele, D. H. Werner, J. P. Turpin, and A. Massa, "Generalized QCTO for metamaterial-lens-coated conformal arrays," *IEEE Trans. Antennas Propag.*, vol. 62, no. 8, pp 4089-4095, Aug. 2014.

[12] G. Oliveri, E. Bekele, M. Carlin, L. Tenuti, J. Turpin, D. H. Werner, and A. Massa, "Extended QCTO for innovative antenna system designs," IEEE Antenna Conference on Antenna Measurements and Applications (CAMA 2014), pp. 1-3, Nov. 16-19, 2014.

[13] G. Oliveri, P. Rocca, M. Salucci, E. T. Bekele, D. H. Werner, and A. Massa, "Design and synthesis of innovative metamaterial-enhanced arrays," IEEE International Symposium on Antennas Propag. (APS/URSI 2013), Orlando, Florida, USA, pp. 972 - 973, Jul. 7-12, 2013.

[14] G. Oliveri, "Improving the reliability of frequency domain simulators in the presence of homogeneous metamaterials - A preliminary numerical assessment," *Progress In Electromagnetics Research*, vol. 122, pp. 497-518, 2012.

[15] M. Salucci, G. Oliveri, N. Anselmi, G. Gottardi, and A. Massa, "Performance enhancement of linear active electronically-scanned arrays by means of MbD-synthesized metalenses," *J. Electromagnet. Wave.*, vol. 0, no. 0, pp. 1-29, 2017 (DOI: 10.1080/09205071.2017.1410077).